Source and metric estimation in the eikonal equation using optimization on a manifold

Jérôme Fehrenbach, Lisl Weynans

Manuscript submitted to
AIMS' Journals
Volume **X**, Number **0X**, XX **200X**

doi:10.3934/xx.xxxxxxx

pp. **X–XX**

SOURCE AND METRIC ESTIMATION IN THE EIKONAL EQUATION USING OPTIMIZATION ON A MANIFOLD

Jérôme Fehrenbach*

Université Paul Sabatier
Institut de Mathématiques de Toulouse
118 route de Narbonne - F-31062 Toulouse Cedex 9, France

Lisl Weynans

Univ. Bordeaux, CNRS, INRIA,
Bordeaux INP, IMB, UMR 5251,
F-33400 Talence, France

(Communicated by the associate editor name)

Abstract. We address the estimation of the source(s) location in the eikonal equation on a Riemann surface, as well as the determination of the metric when it depends on a few parameters. The available observations are the arrival times or are obtained indirectly from the arrival times by an observation operator, this frame is intended to describe electro-cardiographic imaging. The sensitivity of the arrival times is computed from Log_x the log map wrt to the source x on the surface. The Log_x map is approximated by solving an elliptic vectorial equation, using the Vector Heat Method. The L^2-error function between the model predictions and the observations is minimized using Gauss-Newton optimization on the Riemann surface. This allows to obtain fast convergence. We present numerical results, where coefficients describing the metric are also recovered like anisotropy and global orientation.

1. Introduction.

1.1. Context.

The study presented in this article aims to reconstruct from partial measurements the sources locations and the metric associated to an eikonal equation on a manifold. The measurements can be performed either directly on the same manifold, or indirectly, e.g. on another surface surrounding the latter. This problem is closely related to a practical issue in electrocardiology, which is the inverse problem of electrocardiographic imaging (ECGI).

ECGI is a non-invasive imaging modality used to reconstruct the electrical activity of the heart. It combines electrical potential measurements on the torso surface with a geometric description of the heart and torso. Electric measurements are performed on the torso from a dense array of electrodes (typically 250 electrodes) that measure the potential at a high time rate (typically 2 kHz). The geometric description of the torso and heart is obtained through Computerized Tomography (CT) or Magnetic Resonance Imaging (MRI) and thus is personnalized for each patient.

2020 *Mathematics Subject Classification.* Primary: 35F21, 49Q12; Secondary: 35R30.
Key words and phrases. Inverse problem, electrocardiographic imaging, eikonal equation.
The first author is supported by INRIA grant.
* Corresponding author.

ECGI aims at bridging the gap between the classical non-invasive 12-leads ECG that lacks in sensitivity and specificity and the invasive intra-cardiac measurements with catheters.

The determination of electrical activity of the heart can in principle be obtained by solving at each time instant a Cauchy problem for the Laplace equation in the torso volume to reconstruct epicardial potential maps from body surface potential maps. However this problem is extremely ill-posed and an adequate regularization strategy has to be used to deal with this ill-posedness, for example Tikhonov regularization, or by incorporating anatomical knowledge or other a-priori information.

Another strategy consists in using the global information available during the complete measurement time interval, instead of processing each time-step independently. Taking into account the fact that electric potential in the heart are obtained by the propagation of an electric wave is an alternative way of regularizing the inverse problem, by considering information from other time steps. The present work is an attempt in this direction. The electrical conduction in the heart is described by the bidomain model [6] which considers the interaction between intracellular and extracellular media. We consider here the anisotropic eikonal equation, which is a simplified model of propagation of the electrical activation front in its asymptotic regime [11], but yet accurate enough to produce realistic electrograms [25, 20, 21].

The solution T of the eikonal equation is the depolarization time of the heart surface, i.e. $T(x)$ is the arrival time of the activation front at the point x. The equation reads

$$\begin{cases} \|\nabla T\|^2_{D(x)} &= 1, \\ T(x_i^0) &= \tau_i, i = 1 \dots s, \end{cases}$$

where

- the tensor quantity $D(x)$ describes the anisotropic conduction. It accounts for the local fiber orientation that induces an anisotropy in conduction velocity of the cardiac tissue.

- the boundary conditions depict the initialization of the electric front at earliest activation sites, that we will call throughout this paper the sources. In other words a front is initiated at the source x_i^0 at time τ_i. Physiologically, the source x_i^0 is activated by the network of Purkinje fibers.

We consider in the present work only the surface of the heart (epicardial potential) and the domain is viewed as a 2-dimensional manifold equipped with the metric induced by $D(x)$. The formulation of the eikonal equation in this context requires more material and is provided in equation (1).

At this point, let us remark that the aforemetionned electrical reconstructions on the heart surface are used to build activation maps that are used by cardiologists in order to help to diagnose and treat cardiac conditions. In these activation maps some features are particularly interesting to be detected: the earliest sites of electrical activation (and their activation times), and the presence of zones where the front propagation speed is slower. Thus one additional advantage of using an eikonal equation is that these features are naturally parameters of the model.

In this paper, we formulate rather the eikonal equation in the framework of a Riemannian manifold, because this framework is convenient to describe partial differential equations on a surface with local properties. In this case the conductivity is directly taken into account in the metric of the manifold. The inverse problem to solve amounts to identify the sources, their activation times and possibly parameters

of the metric, from direct (on the heart surface) or indirect (on another surface) electrical measurements. In practice, we use a variational approach and minimize a quadratic cost function measuring the mismatch between the observations and the predictions of the model. To this purpose we compute the sensitivity of the arrival times of the eikonal equation with respect to the source locations, and with respect to the metric. The sensitivity with respect to the source locations is obtained by computing Log_x, which is the logarithmic map with respect to the source x on the surface of the manifold. The Log_x map is approximated by solving an elliptic vectorial equation, namely the Vector Heat Method [26]. The sensitivity with respect to the metric is obtained by an algorithmic differentiation based on the computation of the distance map with the Heat method. Using the Heat method and the Vector Heat Method avoids to compute geodesics on the manifold one by one, which would require a much higher computational cost.

1.2. **Related work.** Let us briefly present some recent works that adress similar problems. In [23], the electrical activity of the endocardium is modelled by an isotropic eikonal equation. The objective is to reconstruct the Purkinje network, that provides the earliest activation sites (together with their activation times). The available data are endocardial measures of the arrival times at N sampling points (N of the order of a few 100s). In this work an iterative method adapts the tree-like structure of the Purkinje network in order to increase the number of sampling points where the predictions are close from the measurements. The work [16] considers a bidomain model, which is more accurate than the eikonal approximation. The geometry is a square with horizontal fiber directions, and the sources locations are known. A numerical investigation is performed in order to evaluate the identifiability of the stimulus location and duration, with different measurement models: the extracellular potential is measured either in the domain, or at the boundary or at part of the boundary. The findings are that a local convergence is observed in all cases, using L-BFGS algorithm.

The work [19] adresses source localization, and uses the viscous eikonal equation, where a term $-\epsilon\Delta T$ is added. It is thus a nonlinear elliptic equation. The sources are described by small subdomains ω_i where a homogeneous Dirichlet condition is imposed, therefore it amounts to assume that all the sources are initiated at time $\tau_i = 0$. In this framework, a shape derivative of the cost function (quadratic mismatch between observed and predicted arrival times measured on part of the boundary) is calculated. It requires the solution of an adjoint problem and provides a vector field h that is used to advect the sources in a direction that decreases the objective function.

The work [24] adresses real ECG data processing. The activation time is assumed to satisfy an anisotropic eikonal equation, where the conductivity's principal direction is obtained by a rule-based method excepted at the scars which are identified from MRI images. A derivative-free algorithm is used to iteratively estimate the sources activations times and some electrical parameters, and then sources with small region of influence are removed. Results on a cohort of 11 patients are presented.

The reference that uses the closest approach from ours is [14], where the model is the anisotropic eikonal equation. The quadratic cost function is minimized using an over-relaxed gradient descent, and the location and timing of the sources are estimated. The Log_x map is computed by extracting each geodesic and the heavy

computational load requires the use of a Graphic Processing Unit. The complementary contribution [15] by the same group proposes to estimate the conduction tensor assuming the source is known. The reconstruction is based on the minimization of a cost-function with a Total-Variation-like regularization that tends to align the fibers.

1.3. **Main contributions and organization.** The present paper intends to propose and validate an efficient computational method to solve the inverse problem of location of sources and identification of metric parameters. It is organized as follows: in section 2 we present the continuous problem formulated in the framework of Riemannian manifolds. In section 3 we compute the sensitivity of the arrival times of the eikonal equation with respect to the source locations and to the metric. In section 4 we present our methodology to solve the inverse problem with a least squares minimization using a manifold Gauss-Newton method. In section 5 we provide details about the numerical methods used to compute in practice the sensitivities with respect to the source locations and to the metric and finally in section 6 we present the validation of the method on several test cases.

2. The continuous problem.

2.1. **Notation.** Let $\mathcal{M}$ be a 2-dimensional Riemannian manifold. The tangent space to $\mathcal{M}$ at the point x is denoted $T_x\mathcal{M}$. The inner product $\langle .|. \rangle_x$ on the space $T_x\mathcal{M}$ induces a linear mapping

$$\mathbf{A}(x) : T_x\mathcal{M} \to T_x^*\mathcal{M},$$

such that for any two vectors $v, w \in T_x\mathcal{M}$, the following identity is true:

$$\langle v|w\rangle_x = \langle \mathbf{A}(x)v|w\rangle_{T_x^*\mathcal{M},T_x\mathcal{M}}.$$

The associated norm is denoted $\|v\|_x$. $\mathbf{A}(x)$ is a positive definite matrix, whose coefficients define a metric on $\mathcal{M}$.

On the cotangent space $T_x^*\mathcal{M}$ the inner product is defined, for any two covectors $p, q \in T_x^*\mathcal{M}$, by:

$$\langle p|q\rangle_{T_x^*\mathcal{M}} = (p|\mathbf{A}(x)^{-1}q)_{T_x^*\mathcal{M},T_x\mathcal{M}}.$$

The associated norm is denoted $\|p\|_{T_x^*\mathcal{M}}$.

2.2. **Forward model for one source.** Let $x \in \mathcal{M}$. The arrival time of a front issued from the point x at time $t = 0$ is the unique viscosity solution u [8] of the eikonal equation

$$\|\nabla u(y)\|^2_{T_y\mathcal{M}} = \big(\mathbf{A}(y)\nabla u(y)|\nabla u(y)\big)_{T_y^*\mathcal{M},T_y\mathcal{M}} = 1, \qquad u(x) = 0. \tag{1}$$

Here $\nabla u(y) \in T_x\mathcal{M}$ denotes the gradient of u on the Riemannian manifold, defined as

$$\forall h \in T_y\mathcal{M}, du(y).h = \langle \nabla u(y)|h\rangle_y.$$

Equivalently, the value $u(y)$ is the length of the shortest path $\gamma_{x\to y}$ joining x and y:

$$u(y) = \int_t \|\gamma'_{x\to y}(t)\|_{\gamma_{x\to y}(t)}\, dt. \tag{2}$$

The path $\gamma_{x\to y}$ is the geodesic joining x and y. It achieves the minimum in the following functional:

$$\int_t \|\gamma'(t)\|_{\gamma(t)}\, dt,$$

among all curves parametrized by $t \in [0,1]$.

In order to emphasize that u is the solution of the eikonal equation issued from the point x, we will also write $u = \phi_x$, or use the alternative notation $\phi(x \to y) = u(y) = \phi_x(y)$. It is well known [8, 3] that u is differentiable everywhere, excepted at the point x and at the cut-locus which is the set of points that can be attained by different shortest geodesics with the same length issued from x. The measure of the cut-locus is zero. Moreover the differential of u can be estimated using a variation of the geodesic from x to y [22]. It is given by

$$du(y).h = \frac{\langle \gamma'_{x\to y}(1) | h \rangle_y}{\|\gamma'_{x\to y}(1)\|_y}.$$

But it follows from the formulation in terms of geodesics (2) that x and y play symmetric roles, and therefore if $y \neq x$ is fixed and is not in the cut locus, then $\phi(x \to y)$ is differentiable w.r.t x and

$$D_x\phi(x \to y).h = -\frac{\langle \gamma'_{x\to y}(0) | h \rangle_x}{\|\gamma'_{x\to y}(0)\|_x},$$

where γ is the geodesic joining x and y. This formula can be also found in [14].

This result can be formulated using the Exponential map, and its inverse the Log map, that are defined as follows. For $v \in T_x\mathcal{M}$ there is a unique geodesic γ issued from x with tangent vector $\gamma'(0) = v$, at least for v in a neighborhood of 0. Then by definition

$$\mathrm{Exp}_x v := \gamma(1),$$

in other words $\mathrm{Exp}_x v$ is obtained by following along the geodesic with initial direction v. Conversely, for $y \in \mathcal{M}$ if there is a unique shortest geodesic γ from x to y then by definition

$$\mathrm{Log}_x(y) = \gamma'(0).$$

It follows that for $v \in T_x\mathcal{M}$ and for $y = \mathrm{Exp}_x v$:

$$D_x\phi(x \to y).h = -\frac{\langle v | h \rangle_x}{\|v\|_x},$$

which reads also, for $y \in \mathcal{M}$:

$$D_x\phi(x \to y).h = -\frac{\langle \mathrm{Log}_x(y) | h \rangle_x}{\|v\|_x}.$$

When the front starts from the point x at some instant τ called the activation time of x, then the arrival time $F(y)$ at any point y is simply shifted by the activation time:

$$F(y) = \tau + \phi(x \to y).$$

2.3. **Observation operator.** The observations are obtained from the arrival times map $F = \tau + \phi(x \to .)$. It is continuous on $\mathcal{M}$, even differentiable almost everywhere. We will use the fact that $F \in L^2(\mathcal{M})$.

In a general inverse problem framework the observation operator is given by

$$G : L^2(\mathcal{M}) \to Y,$$

where Y is a Hilbert space equipped with a norm $\|.\|_Y$. Our theoretical derivations will use a general differentiable observation operator G, but in practical cases of interest we will use either of

- $Y = L^2(\omega)$, where $\omega \subset \mathcal{M}$ and G consists in observing u on the subdomain ω,

• when thinking of electrocardiography, $Y = L^2(\omega \times [0,T])$, where ω represents the union of the electrodes, and G consists of determining the signal at the electrodes during the time interval $[0,T]$. The modelling of this map requires the potential of action and the conductivity map between the surface of the heart $\mathcal{M}$ and the torso where the electrodes are located.

As a summary the observations depending on the source location x and the activation time τ are obtained as follows:

$$\begin{array}{ccccc} \mathcal{M} \times \mathbf{R} & \longrightarrow & L^2(\mathcal{M}) & \longrightarrow & Y \\ (x,\tau) & \longmapsto & F(x,\tau) := \tau + \phi(x \to .) & \longmapsto & G \circ F(x,\tau). \end{array}$$

3. Tangent model.

3.1. Sensitivity w.r.t the source location.

In order to compute the sensitivity of the source-to-observations operator, we use the chain rule. The derivative of G depends on the specific choice of G and will be detailed for each example presented in section 6. We focus here on the sensitivity of $F : x \mapsto \phi(x \to .)$ and suppose for the moment that the activation time is $\tau = 0$. We have proved that if $y \neq x$ does not belong to the cut locus, then

$$D_x\phi_x(y).h = -\langle \mathrm{Log}_x(y) | h \rangle_x.$$

This is a pointwise differentiability result, for a fixed point y. It remains to prove the following global differentiability result:

Theorem 3.1. *Let $\mathcal{M}$ be a complete Riemannian manifold, and $x^\dagger \in \mathcal{M}$. Let K be a compact included in the complementary of the cut locus wrt $x^\dagger$. Then the mapping*

$$\begin{array}{ccc} \mathcal{M} & \to & L^2(K) \\ x & \mapsto & \phi_x = \phi(x \to .) \end{array}$$

is differentiable at the point $x^\dagger$, and

$$D_x\phi_x = -\mathbf{A}(x^\dagger)\mathrm{Log}_{x^\dagger}. \tag{3}$$

The proof is based on the use of the Exp_x map as a chart for K and is postponed to the Appendix.

3.2. Case of s sources.

In practice, there may be a (small) number s of sources to identify, as well as the activation time of each source, that is the initial condition. Let us denote these sources $x_1, \dots x_s$ and the activation times $\tau_1, \dots \tau_s$. The equation to be solved is then

$$\|\nabla F(y)\|^2_{T_y\mathcal{M}} = 1, \qquad F(x_i) = \tau_i, i = 1 \dots s. \tag{4}$$

There is a compatibility condition between the different activation times [2, 5], namely for any pair of sources the distance between these sources must be larger than the difference of their respective activation times. Under this condition, the manifold $\mathcal{M}$ can be partitioned into Voronoi regions relative to each of the sources, up to a set of measure zero called the cut locus. The Voronoi region V_i of a source x_i is the set of points that are closer from x_i than from any other source, once the difference in activation times is taken into account. More precisely

$$V_i = \{ y \in \mathcal{M} \,|\, \tau_i + \phi(x_i \to y) < \tau_j + \phi(x_j \to y) \text{ for } j \neq i \}.$$

The solution F of (4) can also be defined by

$$F(y) = \min_{1 \leq j \leq s} \tau_j + \phi(x_j \to y).$$

The Voronoi region V_i is the set of points y where i achieves strictly the min in the equation above.

The modification of the activation time τ_i of the source x_i has the effect of changing the value of F in V_i by adding a constant to F, and also changing the Voronoi region (it grows if τ_i decreases and shrinks if τ_i increases). However the modification of the Voronoi region has an impact that is of second order on the value of F. More precisely, a variation of τ_i of value ϵ induces a displacement of the boundary of the Voronoi region smaller than ϵ, and the value of F in the region in-between (with area $O(\epsilon)$) is modified by a value smaller than ϵ. On the other hand, in V_i (area $O(1)$) the value of F is modified by a value equal to ϵ. Therefore we will neglect the variation of V_i in our numerical computation of the first order derivative.

Similarly, the effect of the displacement of the source x_i affects the value of F in V_i as well as the boundary of V_i. We neglect the second effect in our numerical simulations.

3.3. **Sensitivity w.r.t the metric.** We are also interested in the case where the metric $\mathbf{A}(x)$ is variable. It is hopeless to recover the value of the metric at each point of $\mathcal{M}$, therefore we will assume that the metric depends on a finite number p of parameters $\boldsymbol{\alpha} = (\alpha_1, \dots, \alpha_p)$. The metric at the point x will be denoted $\mathbf{A}_{\boldsymbol{\alpha}}(x)$.

The arrival time u solution of (1) depends also on $\boldsymbol{\alpha}$ and we emphasize this dependence by denoting

$$\phi^{\boldsymbol{\alpha}}(x \to y)$$

the solution with the metric $\mathbf{A}_{\boldsymbol{\alpha}}(x)$.

When the parameters $\boldsymbol{\alpha}$ that define the metric are perturbed in some direction $\boldsymbol{\beta}$, let us study if the quantity

$$D_{\boldsymbol{\alpha}}\phi^{\boldsymbol{\alpha}}(x \to y).\boldsymbol{\beta}$$

can be defined. We have

$$\phi^{\boldsymbol{\alpha}}(x \to y) = \int_{t=0}^{1} \|\gamma^{\boldsymbol{\alpha}\prime}(t)\|_{\gamma^{\boldsymbol{\alpha}}(t)} dt,$$

where $\gamma^{\boldsymbol{\alpha}}$ is the geodesic from x to y for the metric $\mathbf{A}_{\boldsymbol{\alpha}}$. In other words

$$\phi^{\boldsymbol{\alpha}}(x \to y) = \int_{t=0}^{1} \langle \mathbf{A}_{\boldsymbol{\alpha}}(\gamma^{\boldsymbol{\alpha}}(t))\gamma^{\boldsymbol{\alpha}\prime}(t) | \gamma^{\boldsymbol{\alpha}\prime}(t)\rangle^{1/2} dt.$$

When $\boldsymbol{\alpha}$ is perturbed in some direction $\boldsymbol{\beta}$, the geodesic $\gamma_{\boldsymbol{\alpha}}$ is perturbed in some direction δ that depends linearly on $\boldsymbol{\beta}$. We have

$$D_{\boldsymbol{\alpha}}\phi^{\boldsymbol{\alpha}}(x \to y).\boldsymbol{\beta} = \int_t \frac{\langle \mathbf{A}_{\boldsymbol{\alpha}}(\gamma^{\boldsymbol{\alpha}}(t))\gamma^{\boldsymbol{\alpha}\prime}(t) | \delta'(t)\rangle}{\langle \mathbf{A}_{\boldsymbol{\alpha}}(\gamma^{\boldsymbol{\alpha}}(t))\gamma^{\boldsymbol{\alpha}\prime}(t) | \gamma^{\boldsymbol{\alpha}\prime}(t)\rangle^{1/2}} + \frac{\langle D_{\boldsymbol{\beta}}\mathbf{A}_{\boldsymbol{\alpha}}(\gamma^{\boldsymbol{\alpha}}(t))\gamma^{\boldsymbol{\alpha}\prime}(t) | \gamma^{\boldsymbol{\alpha}\prime}(t)\rangle}{2\langle \mathbf{A}_{\boldsymbol{\alpha}}(\gamma^{\boldsymbol{\alpha}}(t))\gamma^{\boldsymbol{\alpha}\prime}(t) | \gamma^{\boldsymbol{\alpha}\prime}(t)\rangle^{1/2}} \, dt.$$

The contribution of the first term vanishes since it is the first variation of the length of the geodesic $\gamma^{\boldsymbol{\alpha}}$ in the direction δ. It remains

$$D_{\boldsymbol{\alpha}}\phi^{\boldsymbol{\alpha}}(x \to y).\boldsymbol{\beta} = \int_t \frac{\langle D_{\boldsymbol{\beta}}\mathbf{A}_{\boldsymbol{\alpha}}(\gamma^{\boldsymbol{\alpha}}(t))\gamma^{\boldsymbol{\alpha}\prime}(t) | \gamma^{\boldsymbol{\alpha}\prime}(t)\rangle}{2\langle \mathbf{A}_{\boldsymbol{\alpha}}(\gamma^{\boldsymbol{\alpha}}(t))\gamma^{\boldsymbol{\alpha}\prime}(t) | \gamma^{\boldsymbol{\alpha}\prime}(t)\rangle^{1/2}} \, dt,$$

which proves that $\phi^{\boldsymbol{\alpha}}(x \to y)$ is differentiable wrt $\boldsymbol{\alpha}$, and the derivative is given by an integral along the geodesic. In our numerical solution, we implemented an algorithmic differentiation of the Heat Method, see Algorithm 3 below. This allows to bypass the tedious computation of "all" the geodesics.

4. **Parameters estimation.** We propose an iterative algorithm to estimate the source location, the activation time and the parameters of the metric. We first detail the approach used for the source location and activation time, since this part involves optimization on a manifold.

4.1. **Location of the source and activation time.** When the metric is fixed, and the source and the activation time are to be retrieved, we proceed using a variational approach. The aim is to minimize the misfit between the observations and the predictions of the model in a L^2 sense. More precisely consider the cost function defined for $(x, \tau) \in \mathcal{M} \times \mathbf{R}$ by

$$J(x, \tau) = \frac{1}{2} \| G(\tau + \phi_x) - g^{\mathrm{OBS}} \|_Y^2. \tag{5}$$

In this writing, x is the location of the source, and g^{OBS} is the vector describing the observations, that can be viewed as

$$g^{\mathrm{OBS}} = G(\tau^* + \phi_{x^\star}) + \eta,$$

where $x^\star$ is the true location of the source, $\tau^\star$ is the true activation time and η is a noise that affects the measurements.

We solve the least square minimization of J by following the approach of Gauss Newton optimization on a manifold sketched in [1]. It is an iterative method where the k-th iterate is denoted (x^k, τ^k). We determine the direction $(v, \eta) \in T_x\mathcal{M}$ that minimizes the linearized model

$$\ell(v, \eta) = \frac{1}{2} \| G(\phi_{x^k}) + D_x(G(\tau^k + \phi_{x^k})).v + D_\tau(G(\tau^k + \phi_{x^k})).\eta - g^{\mathrm{OBS}} \|_Y^2. \tag{6}$$

We estimate the linear term using the chain rule:

$$D_x(G(\tau^k + \phi_{x^k})).v + D_\tau(G(\tau^k + \phi_{x^k})).\eta = DG(D\phi_{x^k}.v) + \eta DG.\mathbf{1}. \tag{7}$$

The first quantity can be explicitly computed when v is given, since we have seen that $D\phi_x(y).v = \langle \mathrm{Log}_x(y) | v \rangle_{T_x\mathcal{M}}$. In practice, we determine $D_x(G(\tau + \phi_x)).v$ for two values of the vector v that form a basis of $T_x\mathcal{M}$, this gives $D_x(G(\tau + \phi_x))$. The second quantity is $DG.\mathbf{1}$ which is known analytically for practical cases of G. Once the linear maps $T_x\mathcal{M} \to Y$ and $\mathbf{R} \to Y$ are known, the minimization of the linear model (6) is a least-squares problem in dimension 3. We denote $(v^\star, \eta^\star)$ its solution.

Following [1] the next iterate in the minimization algorithm is

$$x^{k+1} := \mathrm{Exp}_{x^k}(v^\star), \qquad \tau^{k+1} := \tau^k + \eta^\star.$$

4.2. **Localization of several sources and their activation time.** In the case of a number s of sources, the modification of the location or the activation time of one source affects only its Voronoi region. The linear model (6) is replaced by an analogous expression, where the i-th source affects only V_i.

4.3. **Joint estimation of the metric and source location.** Suppose that in addition to the location of the source and the activation time, one also wishes to estimate the metric. We assume here again that the metric depends on a small number p of parameters: $\boldsymbol{\alpha} = (\alpha_1, \ldots, \alpha_p)$. The cost function to be minimized is now:

$$J(\boldsymbol{\alpha}, x, \tau) = \frac{1}{2} \| G(\tau + \phi_x^{\boldsymbol{\alpha}}) - g^{\mathrm{OBS}} \|_Y^2.$$

The linearized model around $(\boldsymbol{\alpha}, x, \tau)$ in the direction $(\boldsymbol{\beta}, v, \eta)$ is given by

$$\ell(\boldsymbol{\beta}, v, \eta) = \frac{1}{2}\|G(\tau+\phi_x^{\boldsymbol{\alpha}})+D_{\boldsymbol{\alpha}}(G(\tau+\phi_x^{\boldsymbol{\alpha}})).\boldsymbol{\beta}+D_x(G(\tau+\phi_x^{\boldsymbol{\alpha}})).v+D_\tau(G(\tau+\phi_x^{\boldsymbol{\alpha}})).\eta-g^{\mathrm{OBS}}\|_Y^2. \tag{8}$$

The minimization of this least squares problem of dimension $p+3$ leads to the next iterate. It is straightforward to compute when the linear parts are known. We have already given the linear part corresponding to the variables v and η. For the variable $\boldsymbol{\beta}$ the chain rule yields

$$D_{\boldsymbol{\alpha}}(G(\tau + \phi_x^{\boldsymbol{\alpha}})).\boldsymbol{\beta} = DG(D_{\boldsymbol{\alpha}}\phi_x^{\boldsymbol{\alpha}}.\boldsymbol{\beta}).$$

5. Practical Implementation.

5.1. Discretization of the surface.

The manifold $\mathcal{M}$ is discretized as a triangulated surface $\mathcal{M}_h$, composed of a set of vertices $\{i\}$ and a set of edges $\{ij\}$. The metric $\mathbf{A}$ is given in practice by the lengths of the edges of the triangulation. In order to solve the eikonal equation using Fast-Marching methods the triangulation needs to satisfy an acuteness condition, meaning that all the triangles must be acute [17]. We use in the present work the Heat Method to solve the eikonal equation see subsection 5.2, which requires a slightly different geometric condition, namely the triangulation must be Delaunay w.r.t. the considered metric [4, 26].

In order to encode the tangent space $T_x\mathcal{M}$ to some vertex x we choose a reference direction along an edge issued from x. The sum of the angles issued from x is normalized to 2π, see [18]. A tangent vector at x is then encoded as a complex number attached to x. The mass matrix as well as the stiffness matrices of the Laplace-Beltrami and the connection Laplacian operators are assembled following [26].

5.2. Direct problem.

We discretize the space of possible locations for the source x, by imposing that the point x is a vertex of the mesh. The distance map ϕ_x is solved using the Heat Method [9], which requires to assemble the matrix of the Laplace-Beltrami operator on the triangulated surface $\mathcal{M}_h$. The Heat Method relies on a well-known relationship between geodesic distance and heat kernel on a Riemanian manifold [27]. In practice, with the Heat Method, first the heat kernel is solved, then its gradient is normalized to recover the gradient of the distance field, then the distance field itself is reconstructed from this gradient. This procedure circumvents the high accuracy requirements if the distance field was directly reconstructed from the heat kernel.

Algorithm 1 Heat-Method to compute ϕ_x, see [9]

Input: Triangulated surface $\mathcal{M}_h$, metric $\mathbf{A}$, source point x.
Output: ϕ_x the distance map to x.
Assemble the discrete Laplace-Beltrami operator Δ.
Fix some small time $\tau > 0$ and set $u_0 := \delta_x$ (Dirac mass).
Solve for u the implicit Euler equation $(Id - \tau\Delta)u = u_0$.
Evaluate the vector field $X = -\nabla u/|\nabla u|$.
Solve the Poisson equation $\Delta\phi = \nabla \cdot X$.

Note that the change of variable $u = \exp(v/\sqrt{\tau})$ leads to v satisfying

$$-\sqrt{\tau}\Delta v + |\nabla v|^2 - 1 = 0$$

outside the source point. This is exactly the vanishing viscosity solution of the eikonal equation with parameter $\sqrt{\tau}$. The steps in algorithm 1 that construct ϕ from u amount to straighten up the (smooth) vanishing viscosity solution by weakly imposing a gradient of norm 1.

In practice an heuristic is proposed in [9] that uses for u the average between the solutions with homogeneous Dirichlet and Neumann boundary condition. This note does not apply to the examples presented in Section 6 where $\mathcal{M}$ is a sphere or a closed surface hence has no boundary.

5.3. **Numerical derivative w.r.t. the source location.** Following equations (7) and (3), it suffices to compute the discrete Log_x map on $\mathcal{M}_h$ to obtain the sensitivity w.r.t. x. In order to compute the Log_x map, we use the Vector Heat Method [26] which requires the connection Laplacian. We provide here a brief description and a sketch of the algorithm. For a more complete description we refer the reader to [26]. The Vector Heat Method relies on the result that the vector heat kernel on Riemannian manifolds behaves like parallel transport along shortest paths.

The connection Laplacian is a second derivative on vector fields, and is discretized as a complex matrix on the 2-dimensional surface $\mathcal{M}_h$. The Vector Heat Method has the advantage of providing $\mathrm{Log}_x(y)$ for every mesh point y in one solve, and avoids the costly computation of geodesics issued from each point y. This requires the assembly of the (complex valued) stiffness matrix of the connection Laplacian.

Algorithm 2 Vector Heat-Method to compute Log_x, see [26]

Input: Triangulated surface $\mathcal{M}_h$, metric $\mathbf{A}$, source point x, reference unit vector $e_1 \in T_x\mathcal{M}_h$.
Output: Log_x the log map with origin x.
Assemble the discrete connection Laplacian Δ^∇.
Fix some small time $\tau > 0$ and set $Y_0 := \delta_x e_1$ (Dirac mass).
Integrate $\partial_t Y_t = \Delta^\nabla Y_t$ between 0 and τ with $Y(t=0) = Y_0$.
The horizontal vector field is then $H = Y_\tau / |Y_\tau|$.
Define R_0 the discretized radial vector field issued from x.
The radial vector field R is obtained by transporting R_0.
The coordinates (r, φ) of each vertex y are obtained using R, H and the distance map ϕ_x.
Set $\mathrm{Log}_x(y) = r(\cos\varphi e_1 + \sin\varphi e_1^\perp)$.

5.4. **Algorithmic differentiation w.r.t. the metric.** When the metric is also to be recovered, in the case when it depends on the parameters $\boldsymbol{\alpha} = (\alpha_1, \dots, \alpha_p)$, the description of the problem must include the derivative of each edge length w.r.t. each parameter α_k. In this case we compute the derivative of the arrival time ϕ_x w.r.t. to α_k using algorithmic differentiation as follows.

The numerical approximation of the arrival time ϕ_x is computed using Algorithm 1. We use algorithmic differentiation (chain rule) to estimate the derivative of ϕ_x w.r.t. the metric. Let us denote $\mathbf{A}_k = \partial_{\alpha_k}\mathbf{A}$, and we assume that $\mathbf{A}_k$ is given on the computational mesh, as the derivative of the length of each edge. This is the case in our examples where the metric depends on a few parameters through explicit analytic formulas.

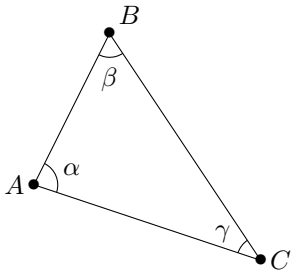

FIGURE 1. Some triangle ABC of the mesh and the associated angles.

The key is to estimate the derivative of the Laplace-Beltrami operator Δ. Let us have more insight on the assembly of Δ as a finite element matrix. For each triangle in the mesh $\mathcal{M}_h$ the contribution to the stiffness matrix is

$$-\frac{1}{2}\begin{pmatrix} b+c & -c & -b \\ -c & c+a & -a \\ -b & -a & a+b \end{pmatrix}$$

where a, b, c are cotangents of the angles of the considered triangle, see Figure 1. The values of the cotangents are related to the lengths of the edges l_{AB}, l_{AC}, l_{BC} using the cosine formula:

$$a = \cot\alpha = \frac{\cos\alpha}{\sin\alpha} = \frac{\cos\alpha}{\sqrt{1-\cos\alpha^2}}, \qquad \cos\alpha = \frac{l_{AB}^2 + l_{AC}^2 - l_{BC}^2}{2 l_{AB} l_{AC}}.$$

From the knowledge of $\partial_{\alpha_k}\mathbf{A}$ one can estimate the derivative of the edge lengths $\partial_{\alpha_k} l_{AB}, \partial_{\alpha_k} l_{AC}, \partial_{\alpha_k} l_{BC}$. Using the above formulas and the chain rule yields $\partial_{\alpha_k} a$. This allows to assemble the derivative of the stiffness matrix $\partial_{\alpha_k}\Delta$, with a contribution in each triangle of the form

$$-\frac{1}{2}\begin{pmatrix} \partial_{\alpha_k} b + \partial_{\alpha_k} c & -\partial_{\alpha_k} c & -\partial_{\alpha_k} b \\ -\partial_{\alpha_k} c & \partial_{\alpha_k} c + \partial_{\alpha_k} a & -\partial_{\alpha_k} a \\ -\partial_{\alpha_k} b & -\partial_{\alpha_k} a & \partial_{\alpha_k} a + \partial_{\alpha_k} b \end{pmatrix}$$

The derivative $\partial_{\alpha_k}\phi_x$ of ϕ_x is obtained with the following algorithm that is obtained by differentiating Algorithm 1:

Algorithm 3 Differentiation of the Heat-Method to compute $\phi' = \partial_{\alpha_k}\phi_x$

Input: Triangulated surface $\mathcal{M}_h$, metric $\mathbf{A}$, derivative $\partial_{\alpha_k}\mathbf{A}$ of the metric, source point x.
Output: $\phi' = \partial_{\alpha_k}\phi_x$ the derivative of the distance map to x.
Assemble the derivative of Laplace-Beltrami operator $\Delta' = \partial_{\alpha_k}\Delta$.
Fix some small time $\tau > 0$ and set $u_0 := \delta_x$ (Dirac mass).
Solve for u the implicit Euler equation $(Id - \tau\Delta)u = u_0$.
Solve for u' the equation $(Id - \tau\Delta)u' = \tau\Delta' u$.
Evaluate the vector field $X' = -\dfrac{|\nabla u|\nabla u' - (\nabla u \cdot \nabla u')\nabla u/|\nabla u|}{|\nabla u|^2}$.
Solve the Poisson equation $\Delta\phi' = \nabla \cdot X'$.

6. **Numerical results.** The test cases 1, 2 and 3 are obtained by direct simulation on a sphere. The anisotropic Riemannian metric is defined using the following 3 parameters: $(\alpha, \kappa, d_\parallel)$ where α is the angle between the principal axis and the meridians on the sphere, κ is the transverse slowness and $d_\parallel$ is the longitudinal slowness.

The simulations were run on a mesh comprising approx. 6000 nodes and 12000 triangles. This mesh was generated using Gmsh [13], and then the Delaunay flip algorithm [10, 4] was applied to obtain a Delaunay triangulation w.r.t. the metric. In order to generate the observations, the anisotropic eikonal equation is solved using AGSI [5]. It is deliberate to use a different method to generate the observations and to solve the inverse problem, this avoids so-called inverse crime [7].

All simulations were implemented with Python 3.7 and run on a laptop equipped with a 2.5 GHz Intel Core i7 processor.

6.1. **Test case 1: localization of a single source.** For this test case the Riemannian metric is defined by the following parameters: $(\alpha = \pi/3, \kappa = 1.8, d_\parallel = 1)$. There is one true point source x^*. The observation operator consists in observing the arrival times on a subset of the mesh vertices composed of 50% randomly selected vertices. The observations are corrupted by an additive Gaussian noise with standard deviation equal to a fraction of the largest arrival time $\|\phi_x\|_\infty$, either 1% (case 1a) or 10% (case 1b).

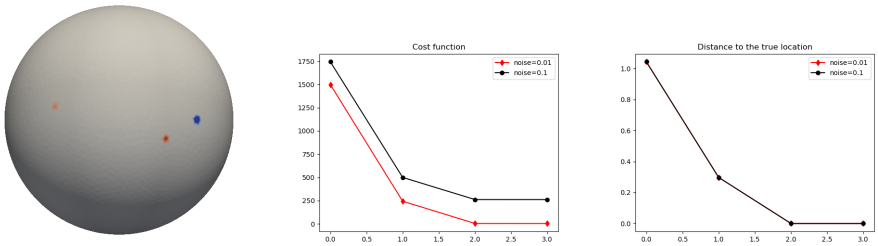

FIGURE 2. Left: location of the successive iterates x^k (red) and the true source point x^* (blue), the 3rd iterate x^3 coincides with x^*. Center: evolution of the cost function J for cases 1a and 1b. Right: evolution of the distance to the solution $\|x^k - x^*\|$ in both cases, note that the iterates are the same for cases 1a and 1b.

The initial position of the source is randomly chosen. We present in Figure 2 the location of the successive iterates, the evolution of the cost function J defined in (5), and the distance of the current iterate to the true location for cases 1a and 1b. We present in Table 1 the estimated activation times. The error is of the order of 0.03, to be compared to the maximum observed arrival time that is about 4.12. Note that in both cases the exact location is retrieved in 3 iterations, and the computational time is approx. 60s.

6.2. **Test case 2: localization of two sources.** For this test case the Riemannian metric is the same as test case 1. There are two point sources x_1^*, x_2^* with respective activation times $\tau_1^* = 0$ and $\tau_2^* = 0.2$. The observation operator consists in observing the arrival times on a subset of the mesh vertices composed of 50% randomly selected vertices. The observations are corrupted by an additive Gaussian

True activation time $\tau^\star$	retrieved τ for case 1a	retrieved τ for case 1b
0.2	0.229	0.217

TABLE 1. Reference and estimated activation times for test case 1

True activation times $\tau_1^\star/\tau_2^\star$	retrieved τ for case 2a	retrieved τ for case 2b
0/0.2	0.031/0.228	0.017/0.226

TABLE 2. Reference and estimated activation times for test case 2

noise with standard deviation equal to a fraction of the largest value $\|\phi_x\|_\infty$, either 1% (case 2a) or 10% (case 2b).

In order to recover two sources, we implemented the splitting method presented in [14]. It consists in starting with one single source, and at each iteration to estimate if an improvement is brought if this source is splitted in two sources. More precisely, we estimate for a number of $N = 20$ angles the modification of the cost function in the Voronoi region of the considered source if a) the source is (infinitesimally) displaced in the given direction b) the source is (infinitesimally) splitted along the given direction. If the gain observed by splitting is more than 5 times larger than the gain observed by moving the source, then it is decided to split the source. We refer the reader to [14] for details, we only emphasize that all the calculations are straightforward once the Log map w.r.t. the considered source is known.

In our implementation, we tried to split the source for the first 4 iterations, then every iteration count that is 2 modulo 5. We also decided to suppress at every iteration any source which has an almost empty Voronoi region (less than 5% of the vertices).

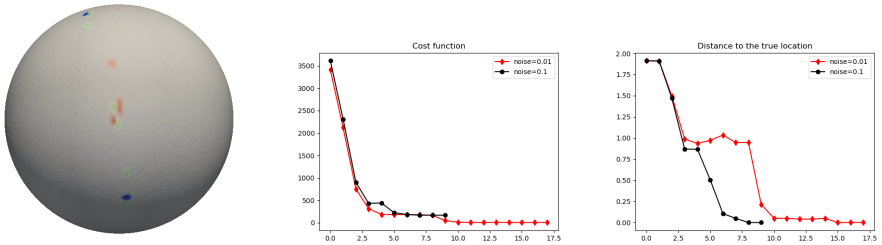

FIGURE 3. Left: location of the successive iterates x^k before splitting (red) and after splitting (green) and the true source points (blue). Center: evolution of the cost function J for cases 2a and 2b. Right: evolution of the distance to the solution in both cases.

The initial position of the source is randomly chosen. We present in Figure 3 the location of the successive iterates, the evolution of the cost function J defined in (5), and the distance to the true sources for cases 2a and 2b. The distance of a set $\{x^k\}$ to the true sources x_1^*, x_2^* is defined as $\max(\min_k \|x^k - x_1^*\|, \min_k \|x^k - x_2^*\|)$. Note that in both cases the exact locations are retrieved. We present in Table 2 the estimated activation times. The computational time is approx. 275s for case 2a (17 iterations) and 140s for case 2b (9 iterations).

6.3. **Test case 3: joint localization of 2 sources and estimation of the metric.** For this test case the Riemannian metric is still defined by the following parameters: $(\alpha = \pi/3, \kappa = 1.8, d_{\|} = 1)$. There are two point sources x_1^*, x_2^*. The observation operator consists in observing the arrival times on a subset of the mesh vertices composed of 30% randomly selected vertices. The observations are corrupted by an additive Gaussian noise with standard deviation equal to a fraction of the largest value $\|\phi_x\|_\infty$, either 1% (case 3a) or 10% (case 3b).

The metric is to be recovered, from an initial guess $(\alpha^0 = \alpha + 0.1, \kappa^0 = \kappa + 0.1, d_{\|}^0 = d_{\|} + 0.1)$. The location of the sources is also to be recovered, starting from one source and applying the same splitting criterion that was used in case 2. In order to stabilize the algorithm, the metric was not optimized during the first 4 iterations, which amounts to ask to modify the metric only when the source(s) point(s) are in a "reasonable" region. We present in Figure 4 the location of the successive iterates, the evolution of the cost function J defined in (5), and the distance to the true sources for cases 3a and 3b. In Figure 5 we show the evolution of the parameters of the metric. We present in Table 3 the estimated activation times.

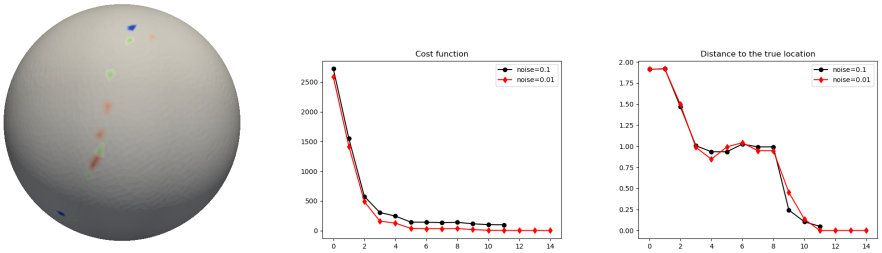

FIGURE 4. Left: location of the successive iterates x^k (red) and the true source point x^* (blue). Center: evolution of the cost function J for cases 3a and 3b. Right: evolution of the distance to the solution $\|x^k - x^*\|$ in both cases.

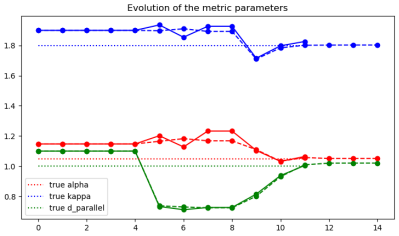

FIGURE 5. Evolution of the parameters of the metric (dashed: case 3a, line: case 3b). Note that it is not optimized during the first 4 steps.

Here again the perfect location of the sources are retrieved. The computational time is approx. 3800s for case 3a (14 iterations) and 3200s for case 3b (11 iterations).

True activation times $\tau^\star$	retrieved τ for case 3a	retrieved τ for case 3b
0/0.2	0.019/0.214	0.011/0.0215

TABLE 3. Reference and estimated activation times for test case 3

6.4. **Test case 4: mimicking an ECG inversion.** In order to demonstrate that our method can be applied to more realistic problems, we present a case where the observations do not take place at the surface itself, but are obtained similarly as electrocardiograms. The surface $\mathcal{M}$ where the eikonal is solved is the surface of the heart, and observations points are located on the surface of the torso. The nonlinear observation operator is constructed as follows. The space for the observations is

$$Y = \{e_1, \dots, e_N\} \times \{t_1, \dots t_M\},$$

where the e_i are electrodes located on the torso, and t_j are observation instants. At the instant t_j the electric potential at the surface of the heart is modelled using a waveform (tanh function) shifted by t_j, applied to the arrival times of the wavefront. This provides a Dirichlet condition on the surface of the heart for a Laplace equation, and the value of the solution at each electrodes minus the value at some reference electrode (first electrode) is the observed potential. The observations are then corrupted by an additive gaussian noise with standard deviation equal to 1% or 10% of the largest observed value.

In this baby simulation that is intended for a proof-of-concept, we used a mesh composed of 4236 points, with 1712 nodes on the surface of the heart. The number of electrodes is $N = 30$ and the number of timesteps is $M = 40$.

We show in Figure 6 the configuration of the electrodes on the torso and the synthetic electrocardiogram for the case of 1% noise. Note that even for such a small value of noise, the measurements are markedly perturbed. We show in Figure 7 the trajectory of the recovered location of the sources, the evolution of the cost function and of the distance to the solution. The estimated activation time is $\tau = 0.163$, while the reference is 0. This error is to be compared with the maximum observed arrival time that is approximately 14.2.

The computational time is about 20 minutes.

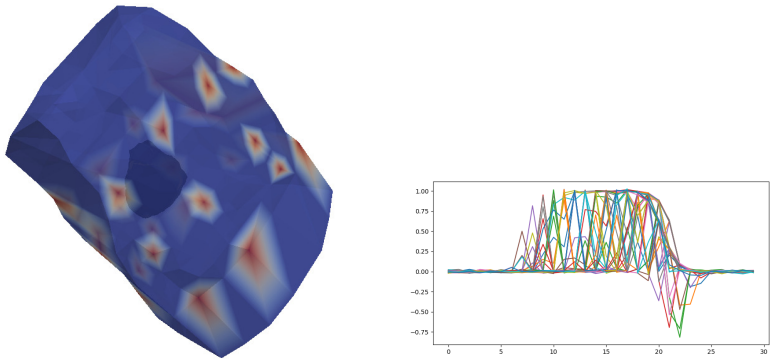

FIGURE 6. Left: configuration of the torso (electrodes in red) and the heart surface (visible by transparency). Right: observations at the electrodes (mimicking an ECG) obtained with noise-level 1%.

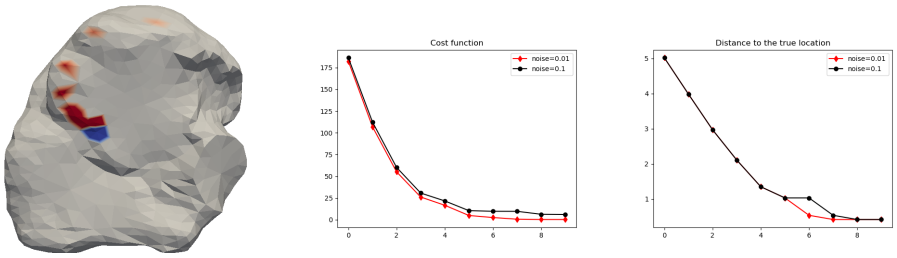

FIGURE 7. Left: location of the successive iterates x^k (red) and the true source point x^* (blue). Center: evolution of the cost function J. Right: evolution of the distance to the solution $\|x^k - x^*\|$ in both cases.

7. **Discussion.** We have proposed a method to locate the sources and retrieve the activation times in the eikonal equation on a manifold, this method also permits to estimate the Riemannian metric in the case it depends on a few parameters. This method converges in a small number of iterations, this is due to the use of Gauss-Newton minimization. In order to compute the Jacobian matrix, we used the Vector Heat Method that allows to obtain the Log_x map rapidly, without a tedious geodesic computation. The solution of the eikonal equation is only approximate but numerical simulations showed satisfactory results. The computation times are orders of magnitude faster than state-of-the-art methods [14], even though our Python implementation was not optimized.

The activation times were in all cases slighlty overestimated. This may be due to the use of the Heat Method that tends to underestimate the distance close to the cut-locus. Therefore it has a bias towards underestimating the time needed to fill the surface, therefore the least-squares fit should tend to overshoot the activation time. This bias is however relatively small in our test cases.

Appendix: proof of Theorem 3.1. Let $\mathcal{M}$ be a complete Riemannian manifold, and let us denote for simplicity $x \in \mathcal{M}$ instead of $x^\dagger$. The cut-locus of x is denoted C_x, and let $U_x = \mathcal{M} \setminus C_x$. Then Exp_x is a diffeomorphism between a star-shaped neighborhood V_x of $0 \in T_x\mathcal{M}$ and U_x [12].

We have thus a chart between V_x and $\mathcal{M}$ minus the cut locus. The Christoffel symbols in this chart are denoted Γ_{ij}^k and are smooth on V_x. This means that the geodesic equation, for any geodesic that does not intersect the cut locus, is described as follows. Let $(\gamma(t))_{t\in[0,1]}$ be the parametrization in V_x of some geodesic, denote $(\gamma^i(t))_{1\leq i\leq 2}$ the coordinates of $\gamma(t)$. Then $\gamma(t)$ is the solution of the following second order ODE:

$$\begin{cases} \dfrac{d^2\gamma^k}{dt^2} + \sum_{i,j} \Gamma_{ij}^k(\gamma(t)) \dfrac{d\gamma^i}{dt}\dfrac{d\gamma^j}{dt} = 0, \\ \gamma(0) = \gamma_0, \\ \gamma'(0) = v_0. \end{cases} \tag{9}$$

The point $\gamma(0) = \gamma_0 \in V_x$ represents the coordinates of the origin of the geodesic, and $\gamma(1)$ the coordinates of its final point in the chart defined by Exp_x.

Consider a compact subset $K \subset U_x$, let $y = \mathrm{Exp}_x w \in K$ for some $w \in V_x$. For $\alpha, \eta > 0$ small enough (to be precised later) we define

$$\begin{array}{rccl} \Gamma: & B(0,\alpha) \times B(w,\eta) & \longrightarrow & V_x \\ & (\gamma_0, v_0) & \longmapsto & \gamma \quad \text{that solves(9).} \end{array}$$

We assume that α, η are sufficiently small so that the geodesic remains in V_x. In words, $\Gamma(\gamma_0, v_0)$ is the geodesic in the parameters domain with starting point γ_0 and initial velocity v_0. Since all the coefficients in (9) are smooth, it follows that Γ is a smooth function of its arguments. We define

$$\Phi(\gamma_0, v_0) = \Gamma(\gamma_0, v_0)(1),$$

it is the endpoint in the parameters domain of the geodesic with starting point γ_0 and initial velocity v_0. For $\gamma_0 = 0$ and $v_0 = v$ we have by definition of the Exp_x map:

$$\Phi(0, v) = v.$$

By smoothness of Φ, for γ_0 sufficiently close from 0 the map $\varphi(\gamma_0) = \Phi(\gamma_0, .)$ defines a diffeomorphism between $B(w,\eta)$ and its image that contains $B(w, \eta/2)$. Up to reducing the value of α, we can assume that for every $\gamma_0 \in B(0,\alpha)$, $\varphi(\gamma_0)$ defines a diffeomorphism between $B(w,\eta)$ and its image that contains $B(w, \eta/2)$.

As a consequence, for every $\gamma_0 \in B(0,\alpha)$ and every $w' \in B(w, \eta/2)$,

$$d_{V_x}(\gamma_0, w') = \int_{t=0}^{1} \|\gamma'(t)\|_{\gamma(t)}\, dt,$$

where $\gamma = \Gamma(\gamma_0, w')$. The notation $d_{V_x}(.,.)$ indicates the distance between points of the parameters domain V_x. All the elements appearing in this formula depend smoothly on γ_0 and w' with bounded derivatives. Therefore the map

$$\begin{array}{rccl} L: & B(0,\alpha) & \longrightarrow & C^1(B(w,\eta/2)) \\ & \gamma_0 & \longmapsto & d(\gamma_0, .) \end{array}$$

is differentiable. This result can be translated in $\mathcal{M}$ as follows: there exist neighborhoods $\mathcal{V}$ of x in $\mathcal{M}$ and $\mathcal{W}$ of y in $\mathcal{M}$ such that the map

$$\begin{array}{rccl} \overline{L}: & \mathcal{V} & \longrightarrow & C^1(\mathcal{W}) \\ & x' & \longmapsto & d(x', .) \end{array}$$

is differentiable. The result is still true if $C^1(\mathcal{W})$ is replaced by $L^2(\mathcal{W})$ because the inclusion $C^1(\mathcal{W}) \subset L^2(\mathcal{W})$ is continuous. The result follows by observing that the compact set K can be covered by a finite number of neighborhoods $\mathcal{W}$.

REFERENCES

[1] P-A Absil, Robert Mahony, and Rodolphe Sepulchre. *Optimization algorithms on matrix manifolds*. Princeton University Press, 2009.

[2] Martino Bardi, Italo Capuzzo Dolcetta, et al. *Optimal control and viscosity solutions of Hamilton-Jacobi-Bellman equations*, volume 12. Springer, 1997.

[3] Guy Barles. *Solutions de viscosité des équations de Hamilton-Jacobi*, volume 17. Springer, 1994.

[4] Alexander I Bobenko and Boris A Springborn. A discrete laplace–beltrami operator for simplicial surfaces. *Discrete & Computational Geometry*, 38(4):740–756, 2007.

[5] Folkmar Bornemann and Christian Rasch. Finite-element discretization of static hamilton-jacobi equations based on a local variational principle. *Computing and Visualization in Science*, 9(2):57–69, 2006.

[6] Yves Bourgault, Yves Coudière, and Charles Pierre. Existence and uniqueness of the solution for the bidomain model used in cardiac electrophysiology. *Nonlinear Analysis: Real World Applications*, 10(1):458–482, 2009.

[7] David L Colton, Rainer Kress, and Rainer Kress. *Inverse acoustic and electromagnetic scattering theory*, volume 93. Springer, 1998.

[8] Michael G Crandall, Hitoshi Ishii, and Pierre-Louis Lions. User's guide to viscosity solutions of second order partial differential equations. *Bulletin of the American mathematical society*, 27(1):1–67, 1992.

[9] Keenan Crane, Clarisse Weischedel, and Max Wardetzky. Geodesics in heat: A new approach to computing distance based on heat flow. *ACM Transactions on Graphics (TOG)*, 32(5):1–11, 2013.

[10] Boris Delaunay. Sur la sphere vide. *Izv. Akad. Nauk SSSR, Otdelenie Matematicheskii i Estestvennyka Nauk*, 7(793-800):1–2, 1934.

[11] Piero Colli Franzone and Luciano Guerri. Spreading of excitation in 3-d models of the anisotropic cardiac tissue. i. validation of the eikonal model. *Mathematical Biosciences*, 113(2):145–209, 1993.

[12] Sylvestre Gallot, Dominique Hulin, and Jacques Lafontaine. *Riemannian geometry*, volume 2. Springer, 1990.

[13] Christophe Geuzaine and Jean-François Remacle. Gmsh: A 3-d finite element mesh generator with built-in pre-and post-processing facilities. *International journal for numerical methods in engineering*, 79(11):1309–1331, 2009.

[14] Thomas Grandits, Alexander Effland, Thomas Pock, Rolf Krause, Gernot Plank, and Simone Pezzuto. Geasi: Geodesic-based earliest activation sites identification in cardiac models. *arXiv preprint arXiv:2102.09962*, 2021.

[15] Thomas Grandits, Simone Pezzuto, Jolijn M Lubrecht, Thomas Pock, Gernot Plank, and Rolf Krause. Piemap: personalized inverse eikonal model from cardiac electro-anatomical maps. In *International Workshop on Statistical Atlases and Computational Models of the Heart*, pages 76–86. Springer, 2020.

[16] Siri Kallhovd, Mary M Maleckar, and Marie E Rognes. Inverse estimation of cardiac activation times via gradient-based optimization. *International journal for numerical methods in biomedical engineering*, 34(2):e2919, 2018.

[17] Ron Kimmel and James A Sethian. Computing geodesic paths on manifolds. *Proceedings of the national academy of Sciences*, 95(15):8431–8435, 1998.

[18] Felix Knöppel, Keenan Crane, Ulrich Pinkall, and Peter Schröder. Globally optimal direction fields. *ACM Transactions on Graphics (ToG)*, 32(4):1–10, 2013.

[19] Karl Kunisch, Aurel Neic, Gernot Plank, and Philip Trautmann. Inverse localization of earliest cardiac activation sites from activation maps based on the viscous eikonal equation. *Journal of mathematical biology*, 79(6):2033–2068, 2019.

[20] Wallman M., Smith N.P., and Rodriguez B. A comparative study of graph-based, eikonal, and monodomain simulations for the estimation of cardiac activation times. *IEEE Trans Biomed Eng.*, 59(6):1739–48, 2012.

[21] Aurel Neic, Fernando O. Campos, Anton J. Prassl, Steven A. Niederer, Martin J. Bishop, Edward J. Vigmond, and Gernot Plank. Efficient computation of electrograms and ecgs in human whole heart simulations using a reaction-eikonal model. *Journal of Computational Physics*, 346:191–211, 2017.

[22] Barrett O'Neill. *Semi-Riemannian geometry with applications to relativity*. Academic press, 1983.

[23] Simone Palamara, Christian Vergara, Elena Faggiano, and Fabio Nobile. An effective algorithm for the generation of patient-specific purkinje networks in computational electrocardiology. *Journal of Computational Physics*, 283:495–517, 2015.

[24] Simone Pezzuto, Frits W Prinzen, Mark Potse, Francesco Maffessanti, François Regoli, Maria Luce Caputo, Giulio Conte, Rolf Krause, and Angelo Auricchio. Reconstruction of three-dimensional biventricular activation based on the 12-lead electrocardiogram via patient-specific modelling. *EP Europace*, 23(4):640–647, 2021.

[25] Maxime Sermesant, Ender Konukoglu, Hervé Delingette, Yves Coudière, Phani Chinchapatnam, Kawal S. Rhode, Reza Razavi, and Nicholas Ayache. An anisotropic multi-front fast marching method for real-time simulation of cardiac electrophysiology. In Frank B. Sachse and Gunnar Seemann, editors, *Functional Imaging and Modeling of the Heart*, pages 160–169, Berlin, Heidelberg, 2007. Springer Berlin Heidelberg.

[26] Nicholas Sharp, Yousuf Soliman, and Keenan Crane. The vector heat method. *ACM Transactions on Graphics (TOG)*, 38(3):1–19, 2019.
[27] Sathamangalam R Srinivasa Varadhan. On the behavior of the fundamental solution of the heat equation with variable coefficients. *Communications on Pure and Applied Mathematics*, 20(2):431–455, 1967.

Received xxxx 20xx; revised xxxx 20xx.

E-mail address: jerome.fehrenbach@math.univ-toulouse.fr
E-mail address: lisl.weynans@math.u-bordeaux.fr